A remarkably air-stable quinodimethane radical cation

Journal:	*ChemComm*
Manuscript ID	CC-COM-06-2020-004025.R1
Article Type:	Communication

COMMUNICATION

A remarkably air-stable quinodimethane radical cation†

Mei Harada, [‡a] Masaru Tanioka, [‡a,b] Atsuya Muranaka,*[c] Tetsuya Aoyama,[c] Shinichiro Kamino[b] and Masanobu Uchiyama*[a,c,d]

Received 00th January 20xx,
Accepted 00th January 20xx

DOI: 10.1039/x0xx00000x

Ambient-stable radical cation of a Thiele's hydrocarbon derivative has been synthesized and its properties have been explored by a combined experimental and computational approach. The radical cation exhibited several intense near-infrared absorption bands and its solution-processed thin films showed high electrical conductivity at room temperature.

Organic radicals with extended π-conjugation have continuously attracted considerable attention due to their unique optical, electronic, and magnetic properties and potential applications in organic electronics, functional dyes, spintronics, and energy storage devices.[1] However, the design and synthesis of air-stable organic radicals having a new molecular skeleton represent an enormous challenge for chemists, since most organic radicals are unstable and highly reactive under air.[2] Herein, we report a new type of air-stable spin-delocalized radical with no bulky protecting groups: bridged-*tetra*-aryl-*p*-quinodimethane (BTAQ) radical cation **1**$^{\bullet+}$ (Fig. 1a). Free radicals often tend to form a spin-paired dimer.[3] Thus, the introduction of bulky substituents is commonly employed to increase the stability, but this approach inevitably hinders intermolecular interactions that are essential for emerging charge and spin transport properties. Spin delocalization with extended π-conjugation is another promising strategy to obtain stable π-conjugated radicals. Tetrathiafulvalene,[4] Wurster's blue,[5] and viologen[6] radical cations are well-known stable radicals without bulky protecting groups and have been widely used in various application fields.

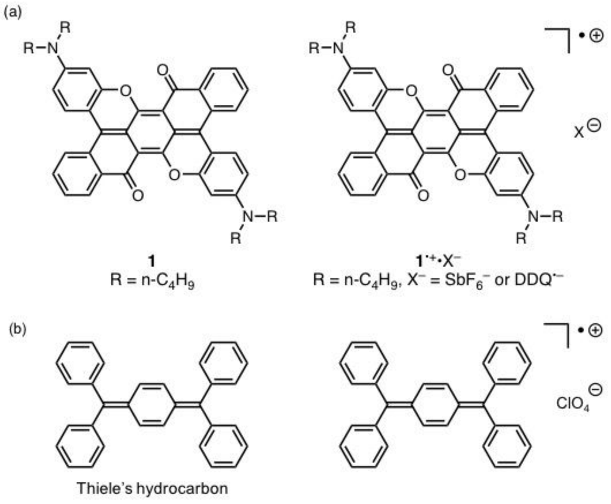

Fig. 1. (a) Bridged-*tetra*-aryl-*p*-quinodimethane (BTAQ) and its radical cation salt. (b) Thiele's hydrocarbon and its radical cation salt.

In the course of our studies on the creation of new functional organic molecules based on fluoran leuco dyes, we recently developed BTAQs as a new family of near-infrared (NIR)-absorbing/emitting dyes.[7] The neutral BTAQ (**1**) can be regarded as a Thiele's hydrocarbon derivative in which two electron-donating aniline groups and two electron-accepting benzoyl groups are incorporated into the π-conjugation of quinodimethane. Although the half-life of Thiele's hydrocarbon radical cation perchlorate (Fig. 1b) is ca. 3 s in CH_2Cl_2 under argon atmosphere,[8] we serendipitously discovered that **1**$^{\bullet+}$ generated by the one-electron oxidation of **1** exhibits intense NIR absorption and extremely high air-stability both in solution and in the solid state under ambient conditions. For instance, chemical oxidation of **1** proceeded smoothly using an equivalent amount of $AgSbF_6$ in CH_2Cl_2 at room temperature. Recrystallization of the product yielded the pure SbF_6 salt (**1**$^{\bullet+}\bullet SbF_6^-$) as a dark olive-green solid in 93% yield. Despite the absence of bulky protecting groups, **1**$^{\bullet+}\bullet SbF_6^-$ is stable in solution and is amenable to silica-gel column chromatography (see Fig. S5 in ESI). Moreover, the isolated powder is air-stable for at least 10 months. Open-shell character of **1**$^{\bullet+}\bullet SbF_6^-$ was confirmed by measuring the ESR spectra.

---

[a] *Graduate School of Pharmaceutical Sciences, The University of Tokyo, Tokyo 113-0033, Japan. E-mail: uchiyama@mol.f.u-tokyo.ac.jp*
[b] *School of Pharmaceutical Sciences, Aichi Gakuin University, Aichi 464-8650, Japan.*
[c] *Cluster of Pioneering Research (CPR), Advanced Elements Chemistry Laboratory, RIKEN, Saitama, 351-0198 (Japan) E-mail: atsuya-muranaka@riken.jp*
[d] *Research Initiative for Supra-Materials (RISM), Shinshu University, 3-15-1 Tokida, Ueda, Nagano 386-8567, Japan*

† Electronic Supplementary Information (ESI) available: experimental procedures, characterization data, and computational details. CCDC 1990118 for **1**$^{\bullet+}\bullet DDQ^{\bullet-}$ and CCDC 1990124 for **1**. For ESI and crystallographic data in CIF or other electronic format see DOI: 10.1039/x0xx00000x

‡ These authors contributed equally.

A single ESR signal was observed for a CH_2Cl_2 solution (g = 2.0035, ΔH_{msl} = 1.02 mT,Fig. 2a) or the powder sample (g = 2.0007, ΔH_{msl} = 1.07 mT, Fig. S2 in ESI) under ambient conditions. Oxidation of **1** was also achieved using 2,3-dichloro-5,6-dicyano-*p*-benzoquinone (DDQ) (see ESI). The cyclic voltammogram of **1** was measured to reveal a very low first oxidation potential (–0.25 V *vs.* Fc/Fc$^+$), which is well correlated with the ease of chemical oxidation (see Fig. S1 in ESI).

Fig. 2b shows the electronic absorption spectra of the radical cations and the neutral form of **1** in CH_2Cl_2 at room temperature. In contrast to the relatively simple NIR absorption of **1** at 829 nm, $\mathbf{1}^{\bullet+}\bullet SbF_6^-$ exhibited several absorption bands at 1303, 1094, 1007, and 927 nm with high extinction coefficients (up to 8.5 × 10^4 M^{-1} cm^{-1}).[9] Time-dependent density functional theory (TDDFT) calculations of a model radical cation ($\mathbf{1_{Me}}^{\bullet+}$) indicated that the spectral features can be correlated with two-dimensionally π-extended structure (see Fig. S3 and Table S1 in ESI). Thus, the 1303 nm absorption band is assigned to the SOMO→LUMO transition, which is polarized to the x-axis, whereas the 927 nm band is attributable to the HOMO→SOMO transition. As the HOMO is localized along the x'-axis, the polarization direction of the HOMO→SOMO transition (x'-axis) is different from that of the π-π* transition between the delocalized SOMO and LUMO (x-axis) (Fig. 2c). The absorption bands at 1160 and 1007 nm appear to be vibronic bands of the SOMO→LUMO transition.[10] The spectral features of the DDQ salt were essentially identical to those of the SbF_6 salt, and the weak absorption bands in the 500-600 nm region are due to DDQ radical anion.[11]

The stability of our radical cation salts in CH_2Cl_2 was examined and compared with that of a commercially available stable radical cation salt, tris(4-bromophenyl) ammoniumyl hexachloroantimonate (Magic Blue, $\mathbf{2}^{\bullet+}\bullet SbCl_6^-$). Fig. 3a shows plots of absorbance at the maximum absorption wavelength *vs.* time under ambient air and room light (fluorescent light) conditions.[12] No absorbance change was observed for $\mathbf{1}^{\bullet+}\bullet SbF_6^-$ after 7 days, which was in marked contrast to the gradual decrease for $\mathbf{2}^{\bullet+}\bullet SbCl_6^-$. $\mathbf{1}^{\bullet+}\bullet DDQ^{\bullet-}$ is somewhat less stable in CH_2Cl_2 than $\mathbf{1}^{\bullet+}\bullet SbF_6^-$, probably owing to the instability of $DDQ^{\bullet-}$ (*vide infra*), but is still more stable than $\mathbf{2}^{\bullet+}\bullet SbCl_6^-$. We also found that our radical cation salts are more persistent than a commercially available neutral π-conjugated stable radical, galvinoxyl radical (see Fig. S6 in ESI).

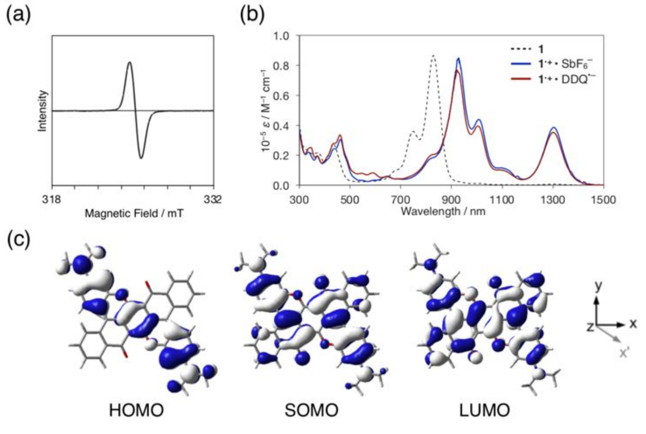

Fig. 2. (a) ESR spectrum of $\mathbf{1}^{\bullet+}\bullet SbF_6^-$ in CH_2Cl_2 under ambient conditions. Modulation amplitude 5.0 mT; modulation frequency 100.00 kHz. (b) Electronic absorption spectra of $\mathbf{1}^{\bullet+}\bullet SbF_6^-$ (blue), $\mathbf{1}^{\bullet+}\bullet DDQ^{\bullet-}$ (red), and **1** (black broken line) in CH_2Cl_2 at room temperature. (c) Frontier molecular orbitals (alpha orbitals) of $\mathbf{1_{Me}}^{\bullet+}$ calculated at the UB3LYP/6-31G(d,p) level.

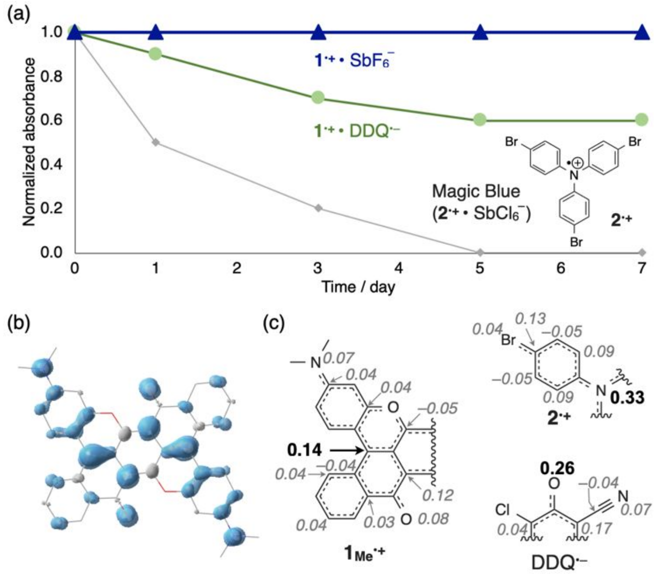

Fig. 3. (a) Effect of storage period on the absorbance of CH_2Cl_2 solutions of $\mathbf{1}^{\bullet+}\bullet SbF_6^-$, $\mathbf{1}^{\bullet+}\bullet DDQ^{\bullet-}$, and Magic Blue ($\mathbf{2}^{\bullet+}\bullet SbCl_6^-$). Each solution was stored under usual room lighting at room temperature. (b) Spin density map (isovalue = 0.002, light blue: positive spin, white: negative spin) of $\mathbf{1_{Me}}^{\bullet+}$ calculated at the UB3LYP/6-31G(d,p) level. (c) Selected Mulliken spin density values of $\mathbf{1_{Me}}^{\bullet+}$, $\mathbf{2}^{\bullet+}$, and $DDQ^{\bullet-}$. Absolute values of more than 0.03 are shown.

To gain insight into the origin of the stability, we calculated the spin densities of $\mathbf{1_{Me}}^{\bullet+}$ and related radicals. As shown in Fig. 3b and 3c, the unpaired electron in $\mathbf{1_{Me}}^{\bullet+}$ is highly delocalized over the π-extended structure including the aniline N atoms and benzoyl O atoms. The highest Mulliken spin density value of $\mathbf{1_{Me}}^{\bullet+}$ was only 0.14, which is much smaller than those of $\mathbf{2}^{\bullet+}$ (0.33) and $DDQ^{\bullet-}$ (0.26), as well as the parent *p*-quinodimethane (Thiele's hydrocarbon) radical cation (0.30; see Fig. S8 in ESI). These results suggest that the intrinsic stability of $\mathbf{1}^{\bullet+}$ arises at least partially from high spin delocalization, and that the stability of the DDQ salt ($\mathbf{1}^{\bullet+}\bullet DDQ^{\bullet-}$) is governed by the less delocalized spin nature of $DDQ^{\bullet-}$.

Unstable or metastable π-conjugated radicals often adopt a dimeric structure called a pancake-bonded dimer, or π-dimer, especially in the solid state.[13] Therefore, we next investigated intermolecular interactions between BTAQ radical cations in the solid state. Although our attempts to obtain single crystals of $\mathbf{1}^{\bullet+}\bullet SbF_6^-$ were unsuccessful, we could obtain single crystals of $\mathbf{1}^{\bullet+}\bullet DDQ^{\bullet-}$ suitable for X-ray diffraction analysis. To our surprise, $\mathbf{1}^{\bullet+}$ has an unusual one-dimensional columnar structure, and does not form a pancake-bonded dimer (Fig. 4a).[14] Two adjacent radical cations are stacked in an antiparallel (head-to-tail) manner with multiple short intermolecular distances (Fig. 4b). Such a stacking structure was not seen in the X-ray structure of neutral BTAQ (**1**) (see Fig. S9 in ESI) and related π-extended quinodimethane radical cations.[2b,2c,10]

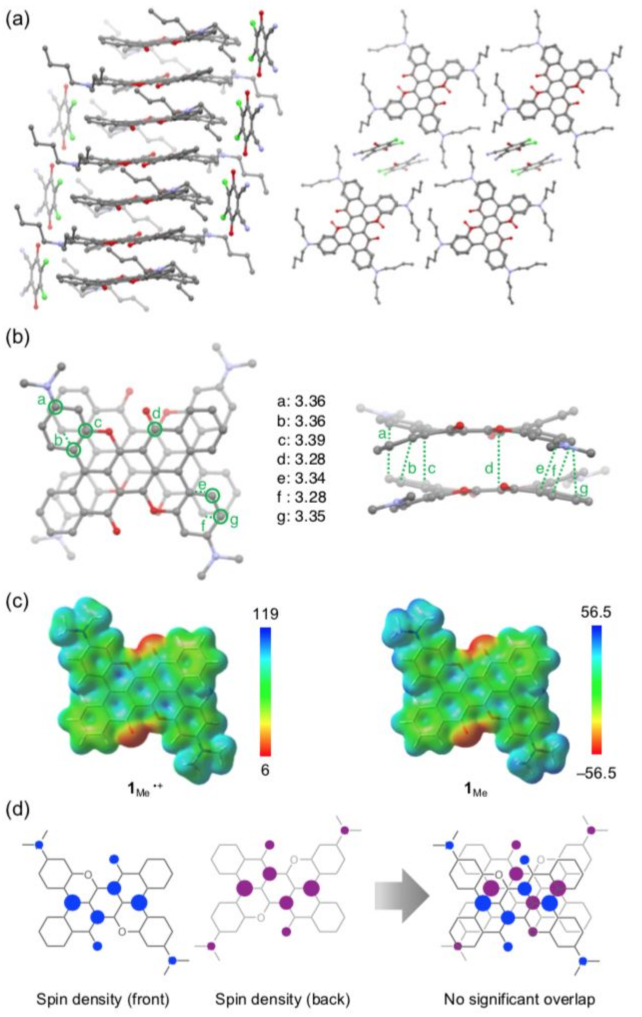

Fig. 4. (a) Crystal packing structures of $\mathbf{1}^{\bullet+}\bullet\mathrm{DDQ}^{\bullet-}$. Solvent molecules and disordered atoms are omitted for clarity. (b) π-Stacking of two adjacent BTAQ radical cations in the X-ray structure. Intermolecular distances less than the van der Waals distance (3.4 Å) are shown in Å. (c) Electrostatic potential (ESP) distributions (isovalue = 0.008) of $\mathbf{1}_{\mathbf{Me}}^{\bullet+}$ and $\mathbf{1}_{\mathbf{Me}}$ calculated at the (U)B3LYP/6-31G(d,p) level. Values are in kcal/mol. (d) Schematic illustration of overlap of spin densities in the two radical cations.

We consider that the unusual equidistant stacking of $\mathbf{1}^{\bullet+}\bullet\mathrm{DDQ}^{\bullet-}$ in an alternating manner arises from the combination of characteristics including the non-planar three-dimensional structure, quadrupolar properties, and weak antiferromagnetic interactions. Fig. 4c shows the electrostatic potential (ESP) distributions of $\mathbf{1}_{\mathbf{Me}}^{\bullet+}$ and a model neutral BTAQ ($\mathbf{1}_{\mathbf{Me}}$). One can see that the quadrupolar properties in the π-skeleton increase upon oxidation (see also Fig. S10). Further, DFT calculations were performed for two adjacent BTAQ radical cations in the X-ray structure (($\mathbf{1}_{\mathbf{Me}}^{\bullet+}$)$_2$), and the results indicate that ($\mathbf{1}_{\mathbf{Me}}^{\bullet+}$)$_2$ has an open-shell character regardless of the functional and basis sets (see Table S3 in ESI). For instance, the triplet state is 3.1 kcal/mol more stable than the singlet state at the UB3LYP-D3/6-31G(d,p) level. The absence of strong antiferromagnetic interactions despite the short intermolecular distance is probably due to the absence of significant overlap of spin densities (Fig. 4d, see Fig. S11 and S12 in ESI).[15]

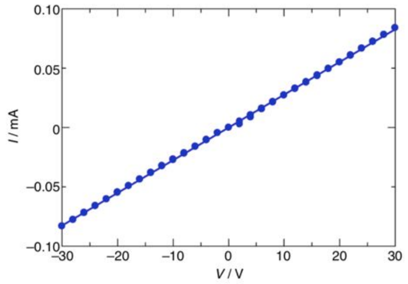

Fig. 5. I/V characteristics of a thin film of $\mathbf{1}^{\bullet+}\bullet\mathrm{DDQ}^{\bullet-}$ at room temperature. The circles indicate the measured values. The straight line was drawn by the least-squares method.

Finally, the charge transport properties of thin-films of $\mathbf{1}^{\bullet+}\bullet\mathrm{DDQ}^{\bullet-}$ were preliminarily examined. Because solution processing is a prerequisite for printed electronics, BTAQ radical cations are a promising candidate for small-molecular conducting materials. Thin-film devices fabricated by spin coating showed a high electrical conductivity of 7.7×10^{-3} S cm^{-1} with ohmic behavior at room temperature (Fig. 5). This is in contrast to the semiconducting properties of neutral BTAQ (**1**), which has a hole mobility of 1.3×10^{-5} cm^2 V^{-1} s^{-1} (see Fig. S13 in ESI). Intermolecular interactions between the BTAQ radical cations ($\mathbf{1}^{\bullet+}$) may play an important role in the high electrical conductivity, since single crystals of DDQ$^{\bullet-}$ with substituted pyridinium cations are insulators (10^{-12}-10^{-13} S cm^{-1}) or semiconductors (10^{-9} S cm^{-1}).[16] As the conductivity is dependent on morphology and counterions,[17] further optimization would lead to better conductivity.

In conclusion, we have discovered a new type of stable π-conjugated radical cation, i.e., bridged-*tetra*-aryl-*p*-quinodimethane (BTAQ) radical cation. Because of the three-dimensionally π-extended *p*-quinodimethane structure including heteroatoms, the radical cation has unique properties: extremely high stability in air under ambient conditions, intense and broad near-infrared absorption, high spin delocalization, a unique one-dimensional columnar structure, and high electrical conductivity. We believe the facile synthesis of highly stable BTAQ radical cations without bulky protecting groups opens up new opportunities for application of stable π-conjugated radical cations, as well as for designing new stable π-conjugated radicals.

This work was partly supported by JSPS KAKENHI(S) (No. 17H06173), JSPS Grant-in-Aid for Scientific Research on Innovative Areas (No. 17H05430), and JST CREST (No. JPMJCR19R2) (to M.U.). HOKUSAI (RIKEN) provided the computer resources for the DFT calculations. Advanced Characterization Nanotechnology Platform (Univ. of Tokyo) provided ESR facilities. We are grateful to Dr. Takashi Matsumoto (Rigaku) and Dr. Kazunori Miyamoto (Univ. of Tokyo) for X-ray analysis. We also thank Dr. Xingmei Ouyang and Ms. Mieko Utsugi (RIKEN) for experimental support.

Conflicts of interest

There are no conflicts to declare.

Notes and references

1 (*a*) O. Hammerich and M. B. Nielsen, *J. Mater. Chem. C*, 2019, **7**, 2809–2822; (*b*) D. W. Zhang, J. Tian, L. Chen, L.

Zhang and Z. -T. Li, *Chem. Asian J.*, 2015, **10**, 56–68; (*c*) M. Hasegawa and M. Iyoda, *Chem. Soc. Rev.*, 2010, **39**, 2420–2427; (*d*) E. Coronado and P. Day, *Chem. Rev.*, 2004, **104**, 5419–5448; (*e*) J. Yamada and H. Akutsu, *Chem. Rev.*, 2004, **104**, 5057–5083; (*f*) Y. Shirota, *J. Mater. Chem.*, 2000, **10**, 1–25.

2 (*a*) B. Tang, J. Zhao, J. -F. Xu and X. Zhang, *Chem. Sci.*, 2020, **11**, 1192–1204; (*b*) G. Xie, V. Brosius, J. Han, F. Rominger, A. Dreuw, J. Freudenberg and U. H. F. Bunz, *Chem. Eur. J.*, 2020, **26**, 160–164; (*c*) C. M. Wehrmann, R. T. Charlton and M. S. Chen, *J. Am. Chem. Soc.*, 2019, **141**, 3240–3248; (*d*) M. Berville, J. Richard, M. Stolar, S. Choua, N. L. Breton, C. Gourlaouen, C. Boudon, L. Ruhlmann, T. Baumgartner, J. A. Wytko and J. Weiss, *Org. Lett.*, 2018, **20**, 8004–8008; (*e*) Q. Qi, P. M. Burrezo, H. Phan, T. S. Herng, T. Y. Gopalakrishna, W. Zeng, J. Ding, J. Casado and J. Wu, *Chem. Eur. J.*, 2017, **23**, 7595–7606; (*f*) T. Nishinaga, Y. Sotome, *J. Org. Chem.*, 2017, **82**, 7245–7253; (*g*) N. Fukui, W. Cha, D. Shimizu, J. Oh, K. Furukawa, H. Yorimitsu, D. Kim and A. Osuka, *Chem. Sci.*, 2017, **8**, 189–199.

3 (*a*) K. Uchida, Y. Hirao, H. Kurata, T. Kubo, S. Hatano and K. Inoue, *Chem. Asian J.*, 2014, **9**, 1823–1829; (*b*) H. Yokoi, S. Hiroto and H. Shinokubo, *J. Am. Chem. Soc.*, 2018, **140**, 4649–4655; (*c*) S. Rösel, J. Becker, W. D. Allen and P. R. Schreiner, *J. Am. Chem. Soc.*, 2018, **140***,* 14421–14432; (*d*) L. Moshniaha, M. Żyła-Karwowska, P. J. Chmielewski, T. Lis, J. Cybińska, E. Gońka, J. Oschwald, T. Drewello, S. M. Rivero, J. Casado and M. Stępień, *J. Am. Chem. Soc.*, 2020, **142**, 3626–3635.

4 (*a*) F. Wudl, G. M. Smith, E. J. Hufnagel, *J. Chem. Soc. Chem. Commun.*, 1970, 1453–1454; (*b*) H. V. Schröder and C. A. Schalley, *Beilstein J. Org. Chem.*, 2018, **14**, 2163–2185.

5 (*a*) C. Wurster and E. Schobig, *Ber. Dtsch. Chem. Ges.*, 1879, **12**, 1807–1813; (*b*) L. Michaelis, M. P. Schubert and S. Granick, *J. Am. Chem. Soc.*, 1939, **61**, 1981–1992; (*c*) A. Ito, Y. Ono and K. Tanaka, *Angew. Chem. Int. Ed.*, 2000, **39**, 1072–1075.

6 (*a*) L. Michaelis, *Biochem. Z.*, 1932, **250**, 564–567; (*b*) L. Michaelis and E. S. Hill, *J. Gen. Physiol.*, 1933, **16**, 859–873; (*c*) T. M. Bockman and J. K. Kochi, *J. Org. Chem.*, 1990, **55**, 4127–4135; (*d*) J. Ding, C. Zheng, L. Wang, C. Lu, B. Zhang, Y. Chen, M. Li, G. Zhai and X. Zhuang, *J. Mater. Chem. A*, 2019, **7**, 23337–23360.

7 Neutral BTAQ with four butyl groups (**1**) was easily synthesized by one-step reaction from 2-(4-dibutylamino-2-hydroxybenzoyl)benzoic acid and 1,4-dimethoxybenzene. Y. Okamoto, M. Tanioka, A. Muranaka, K. Miyamoto, T. Aoyama, X. Ouyang, S. Kamino, D. Sawada and M. Uchiyama, *J. Am. Chem. Soc.*, 2018, **140**, 17857–17861.

8 H. Hart, J. S. Fleming and J. L. Dye, *J. Am. Chem. Soc.*, 1964, **86***,* 2079–2080.

9 The spectral features of $\mathbf{1}^{\bullet+}\bullet\mathrm{SbF}_6^-$ are very similar to those of the product of electrochemical one-electron oxidation of neutral BTAQ with four hexyl groups (see ref. 7).

10 C. Sato, S. Suzuki, K. Okada and M. Kozaki, *Chem. Asian J.*, 2018, **13**, 3729–3736.

11 (*a*) G. Grampp, S. Landgraf and K. Rasmussen, *J. Chem. Soc., Perkin Trans. 2*, 1999, 1897–1899; (*b*) V. Ganesan, S. V. Rosokha and J. K. Kochi, *J. Am. Chem. Soc.*, 2003, **125**, 2559–2571.

12 The normalized absorbance was based on the absorbance at the time of solution preparation. The maximum absorption wavelengths used for $\mathbf{1}^{\bullet+}\bullet\mathrm{SbF}_6^-$, $\mathbf{1}^{\bullet+}\bullet\mathrm{DDQ}^{\bullet-}$, and $\mathbf{2}^{\bullet+}\bullet\mathrm{SbCl}_6^-$ were 1303, 1303, and 728 nm, respectively.

13 (a) M. Kertesz, *Chem. Eur. J.*, 2019, **25**, 400–416; (*b*) X. Chen, B. Ma, X. Wang, S. Yao, L. Ni, Z. Zhou, Y. Li, W. Huang, J. Ma, J. Zuo and X. Wang, *Chem. Eur. J.*, 2012, **18**, 11828–11836; (*c*) T. Devic, M. Yuan, J. Adams, D. C. Fredrickson, S. Lee and D. Venkataraman, *J. Am. Chem. Soc.*, 2005, **127**, 14616–4627.

14 Aggregation does not seem to occur in solution at least under our experimental conditions since the appearance of the electronic absorption spectrum of $\mathbf{1}^{\bullet+}\bullet\mathrm{DDQ}^{\bullet-}$ in CH_2Cl_2 was not altered by changing concentration (see Fig. S4 in ESI).

15 J. P. Peterson, A. Ellern and A. H. Winter, *J. Am. Chem. Soc.*, 2020, **142**, 5304–5313.

16 K. Molcanov, D. Stalke, A. Santic, S. Demeshko, V. Stilinovic, Z. Mou, M. Kertesz and B. Kojic-Prodic, *CrystEngComm*, 2018, **20**, 1862–1873.

17 (*a*) L, Chen, K. S. Mali, S. R. Puniredd, M. Baumgarten, K. Parvez, W. Pisula, S. De Feyter and K. Müllen, *J. Am. Chem. Soc.*, 2013, **135**, 13531–13537; (*b*) G. Heywang, L. Born and S. Roth, *Synth. Met.*, 1991, **41–43**, 10731078.

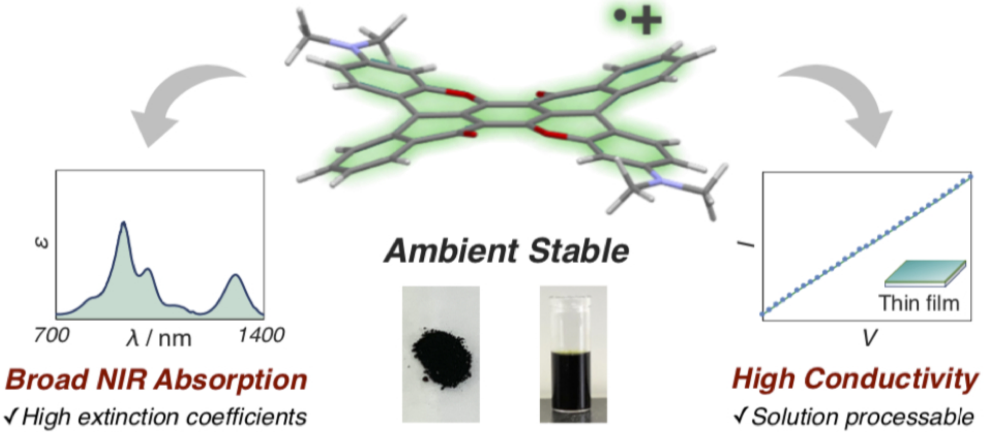

81x40mm (300 x 300 DPI)